Acta Acustica united with Acustica
Vol. 98 (2012) 611 – 628

DOI 10.3813/AAA.918542

Interpreting the Input Admittance of Violins and Guitars

J. Woodhouse, R. S. Langley
Cambridge University Engineering Department, Trumpington St, Cambridge CB2 1PZ, UK. jw12@cam.ac.uk

Summary
The most widespread vibration measurement on musical instrument bodies is of the point mobility at the bridge. Analysis of such measurements is presented, with a view to assessing what range of information could feasibly be extracted from the corpus of data. Analysis approaches include (1) pole-residue extraction; (2) damping trend analysis based on time decay information; (3) statistical estimates based on SEA power-balance and variance theory. Comparative results are shown for some key quantities. Damping trends with frequency are shown to have unexpectedly different forms for violins and for guitars. Linear averaging to estimate the "direct field" component gives a simple and clear visualisation of any local resonance behaviour near the bridge, such as the "bridge hill", and reveals some violins that show a double hill, while viols show only weak hills, and guitars none at all.

PACS no. 43.60, 43.75.Gh

1. Introduction

How much information can be squeezed out of a single vibration measurement on a structure? This question could be of interest for a range of application problems, especially where measurements are difficult and data rare. But in musical instruments there is a more specific reason to ask this question. Any acoustical stringed instrument has vibrating systems with very different properties coupled together at discrete points: the strings and the instrument body. In an instrument like the violin or the guitar, it is generally assumed that the majority of the energy transmission from string to body that eventually leads to sound radiation comes through one end of the string, at the bridge. There is always a significant impedance mismatch between the two coupled systems at this point, otherwise the string would not retain its separate identity sufficiently to produce approximately harmonic overtones, a necessity for a "musical" sound.

This observation leads to the notion that the most useful single measure of the acoustical performance of an instrument might be the input admittance (or point mobility) of the body at the position on the bridge where a string makes contact. This governs the energy flow into the body, and also determines the strength of feedback to the string. In a guitar this feedback determines the frequency-dependent decay rates of the overtones [1], while in a violin it is the main influence on questions of "playability", the detailed response of the nonlinear frictional oscillations to a given bow gesture from the player [2]. The input admittance does not contain any direct information about the radiation of sound, but it is easy to reproduce in different laboratories without issues of room acoustics, it is easy to calibrate, and being a mechanical measurement there is a known functional form for the frequency dependence which allows fitting and parameter extraction. Because of these factors it is a measurement that is commonly made, and a large body of measured data exists. The purpose of this paper is to explore what might be learned by "mining" this body of data.

Strictly, there is a separate input admittance for each string because the coupling points on the bridge are slightly separated. However, one might expect that they would be sufficiently similar that a thorough understanding of one such measurement would shed some light on the others. In the case of a guitar it is relatively simple to measure the admittance for any of the strings, by tapping on the bridge saddle with a small impulse hammer and measuring the velocity response as close as possible to the same point with a laser vibrometer or a very small attached sensor. The most important direction of string motion for excitation of bending vibration in the top plate of the guitar is normal to the plate surface, which is also the easiest direction for measurement of the admittance. Response in the tangential direction also has some influence [1], but it is minor by comparison. It is also much more awkward to measure reliably because there is nothing firm for the impact hammer to strike against to produce broad-band input forcing in that direction.

In the violin this issue of excitation direction is more tricky. The main input force from a given vibrating string is in the plane determined by the bowing direction, dif-

Received 2 September 2011,
accepted 22 April 2012.

ferent for each string but always very approximately parallel to the top plate of the instrument. The high bridge of the violin family allows a force in the bowing direction at the bridge top to be converted into normal forces at the feet of the bridge, which drive the vibration of the top plate. The usual strategy for making a single measurement (e.g. [3]), which gives an approximation to the input admittance for all the strings, involves measuring from one bridge corner to the other. The top part of the bridge has no in-plane resonances within the frequency range of interest here, so its in-plane motion at each frequency can only involve rigid rotation about some instantaneous centre. If that centre lies near the bottom of the bridge, one could visualise the motion as approximately following round the curve of the bridge top.

Were that to be strictly true, the input admittance would be the same for all strings, and it can be measured by hitting with the impulse hammer on one corner, in the direction of bowing of the nearest string, and measuring with a laser vibrometer or a very small accelerometer or other sensor at the other corner, again in the direction of bowing of its nearest string. This is the basis for all the violin measurements that will be shown in this paper. The miniature impulse hammer (PCB 086D80) is mounted on a pendulum fixture of the kind pioneered for violin measurements by Jansson [3]. Signals are collected, typically at a sampling rate around 40 kHz, by a digital data-logger based on a PC. If an accelerometer is used, the result must be integrated in the computer to convert accelerance to mobility. Standard measurement procedures are followed in which repeat impacts are used to obtain an averaged frequency response and the associated coherence function (see for example [4]). Averaging reduces the effect of measurement noise, and coherence gives an indication of linearity and general data quality.

Since the purpose of the measurements is to characterise the body behaviour independent of the string resonances, the measurements are always made with the strings damped. However, to get useful results it is essential that the strings are in place and tuned to their usual playing tensions. The static loading from the string tensions will modify the body vibration behaviour, and, particularly for the violin, the axial stiffness of the strings also plays a part in the overall dynamic stiffness of the body. In any case, for the violin the strings are needed to hold the bridge in place to make the measurements. String damping is typically effected by weaving a piece of thin card through the strings without making contact with the fingerboard. The aim is to damp the strings enough that no pitch is heard when they are plucked, but without adding damping directly to the body modes as would happen if a damper were inserted between the strings and the fingerboard. The influence of string damping on the results, including the effect of the afterlength strings between the bridge and the tailpiece, will be discussed in some detail in later sections. The use of damped strings in the measurements does not by any means imply a belief that sympathetic string vibration is not a significant component of sound quality in a violin or guitar: but it is argued that it is far easier to use computer processing to add the effect of strings to these measurements than it would be to remove their effect from measurements with undamped strings.

The fixture used to hold the instrument during the measurement can also influence the results. Different choices can be made: some aim for "free-free" conditions, other for something more like the way a player holds an instrument, via the chinrest and a soft support representing a hand on the neck. Contact with the main vibrating areas of the body should be avoided so significant damping is not added, and it is useful for quality control to choose a method that allows accurate re-mounting for repeat measurements. This study combines results from different experimenters, using more than one fixture type. No systematic comparison of the effect of these different fixtures is offered here, although this would be a useful topic for further investigation.

The purpose of this paper is to take admittance measurements as just described, collected by a variety of experimenters, and to explore the possibilities for extracting from them a wide range of information about the vibration characteristics of the instruments. The subtext, although one that will not be explicitly followed up in this paper, is that the input admittance should capture a significant fraction of the individual qualities of each instrument, so that variations between instruments seen in these results may give further inspiration to the design of psychoacoustical tests to look for the elusive physical correlates of quality judgements in musical instruments (e.g. [5, 6]).

There are broadly two types of analysis that can be explored: explicit modal analysis, by pole/residue extraction, and band-averaged statistical analysis, which draws upon the insights of Statistical Energy Analysis (SEA) (see e.g. [7, 8]). The relevant theory will be briefly reviewed in the next section. The methods are illustrated by representative results from a violin, then applied to sets of results on different instruments. There is no claim that the particular results shown here represent the best possible use of any of these approaches: rather, the aim is to introduce the different types of information that can be extracted, and to explore the features they reveal. Each separate type of analysis has its own large literature, and indeed its own current research and unsolved problems. It is not possible to encompass all of that here: the more modest aim of this paper is to give an introduction and comparative survey. Even so, some novel and interesting results will be shown, pointing towards promising lines for further research.

2. Theory

2.1. Modal analysis

The input admittance (or drive point mobility) $Y(\omega)$ can be expressed as a modal superposition via a standard formula in terms of the natural frequencies ω_n, modal Q factors Q_n and associated mode shapes u_n. In its simplest form, when damping is assumed to be proportional so that

the mode shapes are real, the result is

$$Y(\omega) = \mathrm{i}\omega \sum_n \frac{u_n^2(\text{bridge})}{\omega_n^2 + \mathrm{i}\omega\omega_n/Q_n - \omega^2}, \quad (1)$$

where u_n^2(bridge) denotes the amplitude of the mass-normalised mode shape at the measurement position on the bridge, in the direction appropriate to the measurement. This mode amplitude relates directly to the "effective mass" of the mode at that point: the equivalent mass-spring-damper oscillator that represents the contribution of that mode to $Y(\omega)$ has a mass $m_n = 1/u_n^2$(bridge). This effective mass will be of the order of the actual vibrating mass when the measurement position is close to an antinode of the mode, but as the measurement position approaches a nodal line the effective mass increases without limit. It should be kept in mind that the normalisation of mode shapes with respect to the mass distribution gives modal amplitude the dimension of mass$^{-1/2}$.

The advantages of modal analysis do not need to be rehearsed in detail here: the vast majority of the existing literature on the acoustics of violin and guitar bodies is concerned with explicit analysis of low-frequency modes. The most elaborate investigations have involved large measurement grids to give good spatial resolution of mode shapes: see especially the "Strad 3D" project [9]. What is not often discussed explicitly in this literature is the reliability of the fitted modal parameters, especially at higher frequencies, but that topic will be important here because the declining usefulness of experimental modal analysis at higher frequencies is the main motivation for seeking additional ways to characterise the response.

The natural way to quantify what is meant by "higher frequencies" here is via the *modal overlap factor*, defined as the ratio of the half-power bandwidth of individual resonances to the frequency spacing between adjacent resonances. When modal overlap is low, each mode contributes a recognisable peak to any frequency response function. When modal overlap is high, at the other extreme, several modes make a significant contribution at a given frequency, and the total response is governed by a summation of these contributions. The result will depend on the relative phases and amplitudes of the various modes. Peaks and dips in a frequency response function will be largely governed by these interference effects, not by individual modes. It is useful to think about individual modes at low modal overlap, but with high modal overlap it is likely to be more appropriate to use a statistical description, dealing in such quantities as average levels, average peak spacings, and typical peak-to-valley heights. The most familiar example occurs in room acoustics. Modal overlap at normal audio frequencies in a moderate or large room is very high, and room acoustics is a statistical science: see for example Cremer *et al.* [10].

Modal overlap tends to increase with frequency. As discussed by Weinreich [11], the modal spacing in an instrument body would be expected to be approximately constant at low frequencies (governed by the bending-plate behaviour of the box) and to decrease at higher frequencies (from the increasing contribution of internal air modes). Modal damping factors usually remain (very approximately) constant with frequency, so that the half-power bandwidth increases roughly linearly with frequency. It follows that the modal overlap, which is low at low frequencies, grows with frequency and eventually becomes large.

The denominator of equation (1) can be factorised,

$$\omega_n^2 + \mathrm{i}\omega\omega_n/Q_n - \omega^2 = -\big(\omega - \Omega_n\big)\big(\omega + \Omega_n^*\big), \quad (2)$$

where for small damping ($Q_n \gg 1$) the complex natural frequency

$$\Omega_n \approx \omega_n\big(1 + \mathrm{i}/Q_n\big), \quad (3)$$

and * denotes the complex conjugate. Equation (1) can then be expressed in partial fraction form, and it is convenient to write the result in the more general form that allows for the possibility of complex mode amplitudes,

$$Y(\omega) = \sum_n \frac{1}{2\Re e\{\Omega_n\}} \left\{ \frac{\Omega_n a_n}{\mathrm{i}\omega - \mathrm{i}\Omega_n} + \frac{\Omega_n^* a_n^*}{\mathrm{i}\omega + \mathrm{i}\Omega_n^*} \right\}. \quad (4)$$

The most general definition of the constant a_n is somewhat complicated (see [12]), but for quite a wide class of linear models for structural damping it relates directly to the complex mode amplitude: $a_n = u_n^2$(bridge). Equation (4) shows that each mode contributes a pair of simple poles to $Y(\omega)$, and standard approaches to pole-residue extraction can be applied to $Y(\omega)$ to fit the modal parameters. There are many techniques for this fitting process, developed in contexts such as system identification and experimental modal analysis (see for example [13]).

Optimal numerical techniques for mode extraction are not the topic of interest here, so for the purposes of this paper a simple approach has been adopted using the Matlab function INVFREQS, which performs rational fraction polynomial approximation, a common method in the field of experimental modal analysis. The frequency response to be analysed is approximated by a ratio of two polynomials, whose roots give the poles and zeros. It is clear from the form of equation (1) or (4), truncated after any finite number of modes, that the denominator polynomial should have order one greater than the numerator polynomial. The particular implementation of the pole-residue extraction method used here is not claimed to be in any sense the "best" approach, but it gives a systematic and automated procedure that will be shown to work moderately well while illustrating the main strengths and weaknesses of the mode-fitting approach. For any particular measurement, it is always possible to achieve a more convincing fit by augmenting the automatic procedure with a little human judgement.

It was found that the best results could be obtained using a fairly low-order model on a series of overlapping frequency bands, rather than attempting a global fit of a high-order model to the entire bandwidth. An analysis bandwidth B is chosen, wide enough to contain several modes

of the system, but not too many. The routine INVFREQS is first applied to the measured $Y(\omega)$ in the range 0–B Hz, with a specified order of the denominator polynomial (and one order less for the numerator). The routine does its best to fit the data in that band using the number of poles and zeros made available by the chosen model order, automatically taking account of the appropriate symmetry property at negative frequencies to guarantee a causal physical system. It will usually choose to put some of the poles outside the analysed band, to represent "residuals", contributions from nearby modes. The analysis band is then advanced by $B/2$ and the process repeated using the data in the range $B/2$–$3B/2$, and so on until the entire bandwidth has been covered for which the data quality is good enough to justify fitting. To avoid double counting of poles, for each analysed band the fitted poles are accepted only if their frequencies lie within the range $B/4$–$3B/4$ relative to the bottom edge of the analysis band in each case: in other words the central half of the analysed band. The first band is an exception: poles are accepted in the range 0–$3B/4$ in that case. There is no equivalent issue for the highest band because the analysed bandwidth always stops short of the Nyquist frequency. Finally, using the full set of deduced poles, the residues are recalculated using a global least-squares fit to $Y(\omega)$ over the entire range.

The result is a list of fitted frequencies, Q factors and "effective masses". In general the fitted residues, and hence the "masses", are complex. This is not physically unrealistic: complex modes are to be expected in systems where the damping is non-uniform in space. This question was first studied by Rayleigh [14], who used a small-damping approximation to obtain expressions for the complex modes of a non-proportionally damped system. His results can be interpreted as saying that significant complexity is expected whenever the modal overlap factor ceases to be very small. This agrees with common experience in experimental modal analysis of any structure: examples from the present study will be shown in section 3. Unfortunately the process of extracting complex modal amplitudes experimentally has been shown to become increasingly ill-conditioned as modal overlap increases, so that the reliability of the fitted phases is questionable [15]. To illustrate this, results will also be shown in which residues are calculated by a least-squares procedure allowing only real values.

2.2. Damping analysis

In contrast to this approach of explicit modal fitting, the measured $Y(\omega)$ can be analysed in a number of ways based on band averaging in the hope of revealing general trends across the frequency range. The first stage is to estimate the damping. This is an issue of some importance in its own right, as well as being an essential stepping stone to the later statistical analysis. Especially for the violin, there is a widespread belief that old instruments, or at least certain old instruments, are better than modern ones. If one is looking for a property of the violin body that might be expected to change with age, damping is a promising candidate. Old wood sometimes acquires a texture quite different from new wood, tending to be crumbly and chalky. This probably points to the presence of micro-cracks in the cell structure of the wood, which might be expected to increase damping (among other things).

Damping trends can be investigated in an analogous way to the measurement of reverberation time as a function of frequency in room acoustics. The approach chosen here uses an inverse Fourier transform of $Y(\omega)$ to give a time series representing the impulse response function, which is then subjected to time-frequency analysis. It may seem roundabout to measure admittance via impulse tests, convert to the frequency domain, then back again to the time domain. However the frequency domain allows averaging to reduce measurement noise, and in any case the great bulk of existing measurements are stored in frequency domain form. A variety of time-frequency analysis algorithms could be applied, but the method adopted is arguably the simplest, involving short-time FFT analysis of successive overlapping segments of the impulse response, shaped with a Hanning window. The characteristics of this approach to structural impulse responses have been explored in detail in an earlier paper [16]. In each frequency band the time decay rate can be estimated by best-fitting an exponential function. A threshold can be specified on the fit quality, measured by the residual mean-square deviation, to filter out poor data points.

The main choice that has to be made in this approach is the length of the individual FFT segments: longer segments give better frequency resolution but poorer time resolution, and shorter segments vice versa. Since damping loss factors for a given system tend to be very approximately constant with frequency, it follows that the decay timescale is usually long at low frequencies and much shorter at high frequencies. Within this broad trend there can also be large local variations. Ideally, the segment length should track this timescale in each frequency band. A simple approach is to analyse each impulse response with a wide range of different segment lengths, and use the fit quality criterion to decide which values to retain from each case. The "good" data points can be combined, and a moving band average can be used to give a single trend line from them all.

If this damping trend is to be regarded as representing the material behaviour of the instrument body, then some account must be taken of the effect of the damped strings, which contribute an extra mechanism of energy loss and will distort the result. Since the admittance has been measured at the coupling point between the strings and the body, there is a simple way to compensate for the effect of the strings. If the string damping is sufficiently high, then they will behave as if they were semi-infinite, taking energy away from the driving point but not returning any of it because it will have decayed to small amplitudes by the time a wave has travelled up and down the string to get back to the bridge. The impedance of a semi-infinite string is the real value $Z_j = \sqrt{T_j m_j}$ where T_j, m_j are the tension and mass per unit length of string j. At the driving

point the impedances of the string and body subsystems simply add, so that if Y_{body} is the true admittance of the body without the additional effect of the damped strings then provided the strings only vibrate in the plane of the measurement,

$$1/Y = 1/Y_{\text{body}} + \sum_j Z_j, \tag{5}$$

where the sum is over all strings connected to the bridge at (or near) the measured point. For a guitar this is simply a sum over the six strings as one would expect. For a violin, each string has a vibrating length on both sides of the bridge, so that if all of these are damped then the sum should be taken over eight semi-infinite strings, not four. Equation (5) can be used to deduce Y_{body} from the measured Y.

The final twist in this story concerns the two polarisations of string motion. Strictly, both the body and the strings need to be represented by a 2×2 matrix of admittances or impedances, to allow for 2D motion in the plane perpendicular to the string axis. The impedance matrix for a string is Z_j times the unit matrix, while for the body all four terms of the matrix are non-zero. The measurement only gives one diagonal term of this matrix. There is an equivalent formula to equation (5) involving these matrices and their inverses, so that if the full matrix for the body was measured, a complete compensation for string damping could be carried through. However, such full measurements are rare [1, 17] and with incomplete knowledge of the matrix full compensation cannot be done. It might be anticipated that some errors will arise from this omission, perhaps by underestimating the full effect of string damping by ignoring energy loss in the second polarisation. This point will be discussed further in the light of measurements in later sections: the effect of this compensation for string damping will be illustrated directly in Figure 15.

2.3. Statistical analysis

Having obtained a damping estimate, further analysis can be carried out based on energy considerations inspired by SEA methods. This is done in the expectation, to be confirmed in results to be shown in the next section, that the automated pole-residue extraction described in section 2.1 will become very unreliable at high frequency, especially once the modal overlap factor becomes significant. Analysis methods like SEA were developed specifically to tackle the corresponding issue in vibration prediction: at high frequency the modal parameters become so sensitive to differences between the actual structure and the nominal one, or between different realisations of the same nominal structure, that deterministic methods like finite-element analysis become much less useful (see for example [18]) and it is more fruitful to consider the ensemble statistics of a set of related but randomly perturbed systems.

The analysis to be presented here is very simplistic, to give a first indication of the kind of things such methods might show. SEA is normally concerned with energy flow between coupled substructures. The central idea behind the method is that, under certain conditions, the *mean energy per mode* in a given subsystem plays a role analogous to temperature in the analysis of heat flow between a system of coupled thermal masses. The rate of energy flow across a junction is proportional to the difference of "temperature", with a proportionality constant known in SEA as the "coupling loss factor". The *modal density* of a subsystem, the mean number of modes per unit frequency interval, plays the role of the heat capacity and is a key parameter of the theory. For a systematic account of SEA, see the text book of Lyon and De Jong [7].

SEA has been extended by a recently-developed hybrid theory that allows it to be combined consistently with finite-element analysis, so that each method can be used where it is most appropriate [19, 20]. It might be very interesting to apply SEA or the hybrid method systematically to, for example, a violin body, but nothing so sophisticated will be considered here: the whole violin, guitar or whichever instrument is being studied will be treated as a single subsystem. The theory behind SEA then gives information about the mean and variance of the response under three kinds of averaging: spatial and frequency averaging, and also ensemble averaging over systems with the same nominal behaviour but random differences of detail. This will allow estimation from the measured input admittance of several quantities, such as the modal density, that might turn out to give useful information of a different character from the results of modal analysis. The necessary underlying theory takes its simplest form for systems with spatially uniform properties. The expected scope and limitations of this approach, given that a musical instrument body does not have such uniform physical properties, will be discussed in later sections once some results have been shown.

Consider a single structural component, such as a plate or shell, subjected to harmonic excitation acting at a single point. The response can be considered to have two components: a direct field and a reverberant field. The direct field corresponds to the outgoing wave response that would be produced by forcing an *infinitely extended* system: direct visualisation of the direct field in a violin has been provided by the transient holographic studies of Molin *et al.* [21, 22]. The reverberant field corresponds to the combined effect of all reflections of the direct field from discontinuities such as joints or edges. Thus write

$$Y(\omega) = Y_{\text{dir}}(\omega) + Y_{\text{rev}}(\omega). \tag{6}$$

The phase of the reverberant response will vary in an irregular way with frequency, as the interference effects between different wave paths change, and it may therefore be reasonable to expect that Y_{rev} will average to zero over a frequency band of sufficient width so that

$$Y_{\text{dir}}(\omega) \approx \left\langle Y(\omega) \right\rangle_\Delta, \tag{7}$$

where $\langle ... \rangle_\Delta$ represents an average taken over a frequency band of width Δ, centred on ω. It can be expected that Δ

will need to contain several modes of the system to average out the reverberant component of the response. In practice it is useful to compute this average using a Hanning window to minimise distracting artefacts as strong features enter or leave the averaging band.

The next stage of analysis is to examine the consequence of balance between power injected by the drive force and the rate of dissipation. Under harmonic excitation at frequency ω with force amplitude F, the time-averaged power input to the system is given by

$$P_{\text{in}} = F^2 \Re e\{Y\}/2. \tag{8}$$

It is a standard SEA result that [7]

$$\left\langle P_{\text{in}} \right\rangle_\Delta \approx F^2 \frac{\pi n}{4M}, \tag{9}$$

where n is the modal density (the inverse of the average mode spacing expressed in rad/s) and M is the total mass. This result follows from approximating the frequency band integral by including only those modes whose frequency falls within the band, and then evaluating the individual modal contributions by taking the integral over the whole range from zero to infinity, on the assumption that the modal bandwidth is much less than the averaging bandwidth. Note that the result is independent of the modal damping factor, and the factor M enters via the average value of the mass-normalised mode amplitude. Both the quantities n and M scale proportional to the linear dimensions of the system, and thus equation (9) is independent of the system size: in fact the equation gives the power into an infinite system, associated with Y_{dir} from the discussion above. Equations (7)–(9) thus yield

$$\Re e\left\{ \left\langle Y(\omega) \right\rangle_\Delta \right\} = \frac{\pi n}{2M}. \tag{10}$$

The energy dissipated by the system can be written as

$$P_{\text{diss}} = \omega \eta E, \tag{11}$$

where η is the loss factor and E is the vibrational energy, which is given by

$$E = \frac{1}{2} \int v^2 \, \mathrm{d}m, \tag{12}$$

where the spatial integral is taken over the whole system, weighted by the local mass dm. For a system with uniform mass distribution this result can be written

$$E = M \overline{v}^2/2, \tag{13}$$

where $\overline{v}^2$ is the space-averaged squared velocity. Equations (12), (13) are based on the assumption that the potential energy is equal to the kinetic energy, and so the total energy is equal to twice the kinetic energy; a factor of 1/2 appears because the current concern is with time-averaged second-order quantities under harmonic excitation.

For most structures with damping levels that are not too high, the reverberant field dominates over the direct field (except very close to the driving point where the direct field may be singular). So the reverberant field at the measured point gives an estimate of $\overline{v}^2$. However, there is a slight twist: it has recently been found that the reverberant field shows (surprisingly) a systematic concentration at the drive point [8] so that the correct estimate takes the form

$$\left\langle \overline{v}^2 \right\rangle_\Delta \approx F^2 \left\langle |Y_{\text{rev}}|^2 \right\rangle_\Delta / K, \tag{14}$$

where the concentration factor K varies from 3 at low modal overlap to 2 at high modal overlap – a reasonable approximate single value is thought to be $K = 2$. Since the power input must equal the power dissipated, equations (11)–(13) yield

$$\frac{\omega \eta M F^2}{2K} \left\langle |Y_{\text{rev}}(\omega)^2| \right\rangle = \left\langle P_{\text{in}} \right\rangle_\Delta. \tag{15}$$

Hence it follows from equations (9) and (10) that

$$\frac{\Re e\left\{ \left\langle Y(\omega) \right\rangle_\Delta \right\}}{\left\langle |Y_{\text{rev}}(\omega)|^2 \right\rangle_\Delta} = \omega \eta M / K. \tag{16}$$

Since the damping trend $\eta(\omega)$ has already been estimated, this equation allows an estimate of the total mass M, and then equation (10) gives an estimate of the modal density n.

An alternative approach to estimating these parameters comes from a slightly unexpected direction, from theoretical results relating to the relative variance of the reverberant field at the drive point. Variance estimation was first considered by Lyon [23], but the result he obtained is in need of correction [8]. The analysis relies on a remarkable property of random vibrating systems, first discovered by numerical experiments and only recently proved [24]. Making any change to a structure alters the vibration frequencies in a way that is particular to that structural change. However, it is found that when the statistical distribution of frequencies is examined, a kind of universal behaviour emerges. Provided the ensemble of perturbed systems has sufficient randomness, regardless of its detailed source, the statistical properties of the natural frequency distribution converge to those associated with a particular family of random matrices called the Gaussian Orthogonal Ensemble (GOE). GOE statistics have been studied in great depth (see e.g. [25]), and results from that study are used to derive SEA variance estimates. The universality of statistical behaviour allows such estimates to be made without needing to specify the nature of the variations within the ensemble of systems.

When this variance theory is applied to the power input or the total energy, both quantities have the same relative variance as $\Re e\{Y\}$, given by

$$\text{Relvar}\big(\Re e\{Y\}\big) = \frac{\alpha - 1}{\pi m}, \tag{17}$$

where Relvar represents the relative variance and $m = \omega \eta n$ is the modal overlap factor. The parameter α is defined in

terms of ensemble averages of mode shapes by

$$\alpha = \frac{E(u_n^4)}{[E(u_n^2)]^2}. \tag{18}$$

If the statistics of the mode shapes are Gaussian the value should be $\alpha = 3$ [8]. Equation (18) strictly relates to the ensemble statistics of the admittance, when the structure is considered to have random properties. However, if the statistics are assumed to be ergodic, then the relative variance can be estimated by frequency averaging, so that

$$\frac{\left\langle \left(\Re e\{Y\} - \langle \Re e\{Y\} \rangle_\Delta \right)^2 \right\rangle_\Delta}{\left\langle \Re e\{Y\} \right\rangle_\Delta^2} \approx \frac{\alpha - 1}{\pi m} \approx \frac{2}{\pi m}. \tag{19}$$

This equation gives a direct estimate of the modal overlap factor m from the measured admittance, without requiring separate knowledge of the damping factor. Eliminating M and η from equations (10) and (16) gives an alternative estimate for m in terms of $|Y_{\text{rev}}|^2$, and it can be shown that the two estimates become equal if

$$\left\langle \Re e\left\{ Y_{\text{rev}} \right\}^2 \right\rangle_\Delta = \left\langle \Im m\left\{ Y_{\text{rev}} \right\}^2 \right\rangle_\Delta \tag{20}$$

which would be true if, for example, the phase of Y_{rev} has a uniform probability distribution. The derivation of equation (19) requires fewer assumptions and so might be more robust when applied to a complex and inhomogeneous object like a musical instrument body. The entire SEA analysis presented here is very well supported by Monte Carlo numerical simulations for single or coupled homogeneous systems, and indeed by experimental validations (see for example [25, 26]), but there are open research questions regarding enhancements that may be needed for best application to inhomogeneous systems. Some synthesised results for an inhomogeneous system will be shown shortly, alongside results for real instruments.

2.4. Sound radiation

Before that, it is useful to enquire briefly whether anything at all can be deduced about radiated sound from a measurement of input admittance alone. No complete answer is possible, of course, but two possibilities present themselves for partial information. The first is a simple but crude argument based on radiation efficiency. It is a common observation (see for example [27]) that the radiation efficiency of most structures tends towards a plateau at high enough frequencies, with a value of the order of unity. When that happens, the total radiated sound power from the structure follows that of an ideal baffled circular piston with the same mean-square surface velocity. Since $\overline{v}^2$ has already been estimated in equation (13), a rough and ready high-frequency estimate of total radiated sound power follows directly.

The second approach to sound radiation is a low-frequency approximation that is specific to musical instrument bodies. A model for the low-frequency function of the guitar from Christensen and Vistisen [28] can be extended to other instruments and a larger number of modes. This lumped-parameter mass-spring-piston model has much in common with the usual treatment of a bass-reflex loudspeaker enclosure. There could be enough information in the bridge admittance, perhaps augmented by some additional information such as the volume of the body cavity, to determine the parameters of such a model. If that could be done, the model could be used to give a prediction of the corresponding sound radiation response at low frequency. This may be a fruitful avenue for further research, but is not pursued here.

3. Sample results

3.1. Modal fitting

To see what all this analysis amounts to, the full set of deduced information will be shown for a single input admittance measurement, of a violin made by David Rubio in 1992. This particular input admittance was measured by the first author using a laser vibrometer and a supporting fixture crudely emulating the hold of a player, employing a chin-rest clamp and a soft support under the centre of the neck. Some results will then be shown from performing the identical analysis on synthesised data, using a model of a "cigar box violin" previously developed for a study of the violin's "bridge hill" and described in detail by Woodhouse [29]. In section 4 some representative comparisons will be shown between different types of instrument, and different instruments of the same type.

The first stage is the modal extraction by pole-residue fitting. It is by no means clear *a priori* what model order and analysis bandwidth to choose for this process. To explore this, five different bandwidths B (300, 400, 500, 600 and 700 Hz) and five different model orders (denominator polynomial of order 10, 12, 14, 16 and 18) were tried. For each set of poles thus obtained, the best sets of complex and real residues were found by minimising the mean of the modulus-squared deviation between measurement and reconstruction. This measure emphasises the fit near the peaks, but does not necessarily take much account of the antiresonances. To give a measure that perhaps corresponds better to what looks like a "good fit" when examining a log-magnitude plot, another measure was then computed, the RMS deviation between the dB levels of the prediction and the measurement. The bandwidth-order combination giving the minimum value of this second measure was selected as "best", evaluated separately for complex residues and real residues. The bandwidth for pole-residue fitting and for evaluating the RMS deviation was 4 kHz.

The number of poles fitted by this process is invariably found to increase systematically as model order goes up and bandwidth goes down. However, the fit quality does not by any means vary in such a simple manner. Figure 1 shows the RMS dB deviation against the number of fitted poles. There is considerable scatter with no clear trend. For this particular example the complex fits (stars) usually do better than the real fits (circles), but this is not universally the case. The best fit is obtained with 84 poles

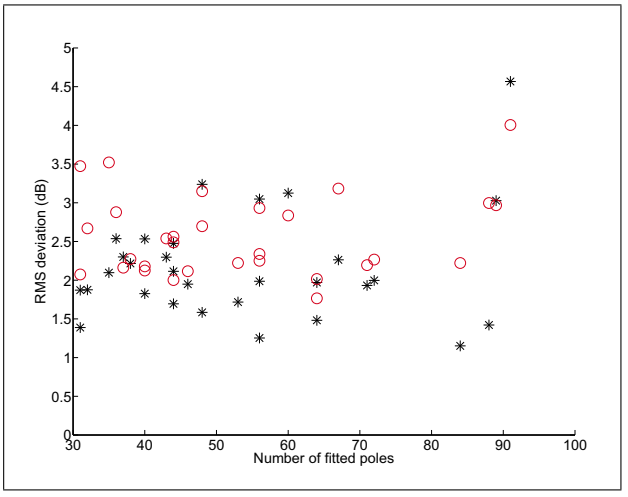

Figure 1. Relation between number of fitted poles up to 4 kHz and quality of fit for the test violin. Fit is measured by the RMS dB deviation between measurement and reconstruction. Stars: results for complex residues; circles: results for real residues.

with complex residues, or 64 poles with real residues, up to 4 kHz. Across the many different instruments analysed in this way, no simple pattern was found that would allow a model order and bandwidth to be selected ahead of time, so this exhaustive search approach is used throughout. The wide range in pole count seen in Figure 1 gives a warning that any attempt to deduce modal density directly from any fitting process of this general kind is likely to be unreliable, although methods of order selection have been proposed that may go some way to circumventing this difficulty (e.g. [30]).

Using the best processing combinations thus selected, the overall quality of fit to the measurement is shown in Figure 2. The best fits with complex and real residues are both shown, to illustrate some of the variation underlying the results in Figure 1. The figure shows both dB magnitude and the real part, for reasons to be explained shortly. The general level of agreement over the whole frequency range is good, but careful examination shows that some peaks are missed by the fitting process in one or both reconstructions.

Figure 3 shows the phases (expressed in degrees) of the fitted residues for the two cases plotted in Figure 2. For the nth pole in isolation, provided that damping is small the peak response occurs at $\omega = \omega_n$ and from equation (4) the peak height is then given by the magnitude of the residue multiplied by Q_n/ω_n. Symbol sizes have been scaled proportional to this peak height expression to give an indication of the importance of each pole. A minimum size is imposed to ensure that poles of small magnitude do not get lost entirely from the plot. Note that INVFREQS fits poles and residues as a function of $i\omega$, rather than of ω, so positive real residues are what equation (4) predicts when the mode shapes are real.

This plot emphasises the difference between the real and complex fits, and immediately gives insight into the ill-

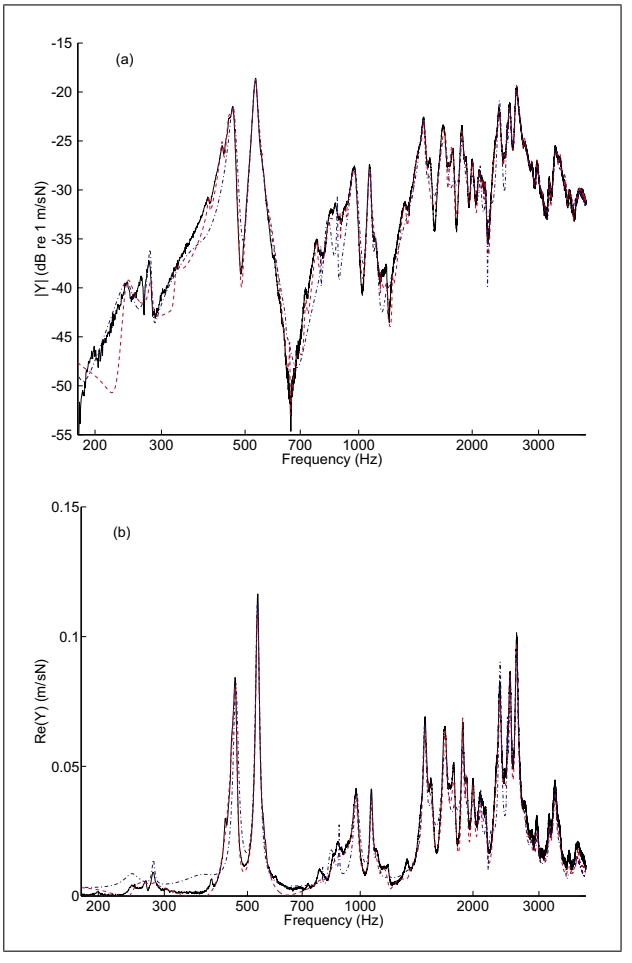

Figure 2. Bridge input admittance for the test violin plotted as (a) magnitude and (b) real part as measured (solid line); reconstructed from pole-residue extraction for the best case with complex residues (dashed line); and reconstructed for the best case with real residues (dash-dot line).

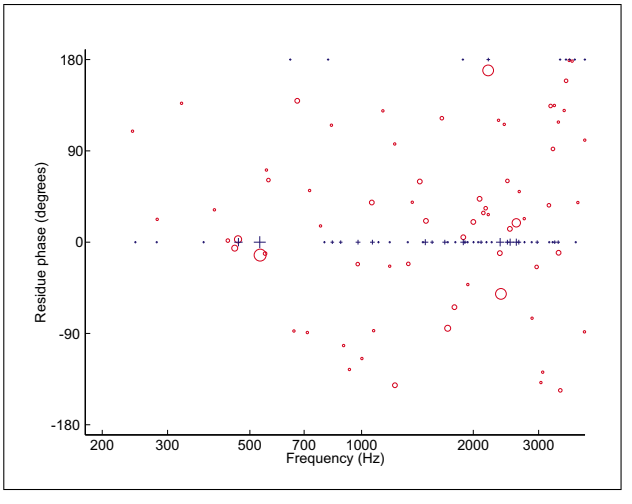

Figure 3. Phase of residues for the poles fitted to the admittance of the test violin, for the best case with complex residues (circles) and the best case with real residues (crosses).

conditioned nature of the process of extracting residues. The general quality of fit is comparable for the two cases,

but it is clear that the pattern of residues is very different. As has already been explained, the true values of the residues would be expected to be somewhat complex at low frequencies, and increasingly complex as the modal overlap increases at higher frequencies. However, the degree of complexity shown here goes beyond the bounds of physical plausibility. The driving-point response of a single mode cannot have a phase outside the range ±90° and still be energetically passive. The complex values are spread over the entire range of phase, and many of the real residues have also come out to be negative (phase 180°), violating the same constraint. These residue fits must be treated with a good deal of scepticism, and that conclusion is not restricted to this particular approach to pole-residue extraction: the ill-conditioning is inherent in the problem, and will be present in any fitting procedure. A modal grid in which transfer functions are measured at many positions will help somewhat in extracting a "best" set of poles, because individual poles may show more clearly at some positions than others, but as modal overlap gets higher the underlying problem of ill-conditioning of residue extraction remains the same.

A slightly different view on the phase of residues is given by looking directly at the real part of the measured $Y(\omega)$, shown in Figure 2b with the two fits. This quantity must remain positive over the whole frequency range, a fact that is commonly used as a check on the quality of a measurement since, for example, any time delay or phase error in the electronics of the measuring equipment very readily disturbs this behaviour. Notice that both fits satisfy this constraint: complex residues, even outside the range determined by the passivity condition, do not necessarily reveal themselves in the phase of the reconstructed admittance.

3.2. Damping results

Next, the extraction of damping information is examined. Figure 4a shows as discrete symbols the individual values resulting from the time-frequency analysis technique described in section 2.2. The processing details are as follows. The sampling rate is 40 kHz for this particular measurement. Sonograms (or spectrograms) were computed with a wide range of lengths of the individual FFTs: 32, 64, 128, 256, 512 and 1024 samples. In each case 30 FFTs were taken, spaced apart by ¼ of the FFT length in all cases. Points were deemed acceptable, and thus plotted here, if at least 6 values were obtained above the noise floor of the measurement, and provided the dB decay showed sufficient linearity as measured by a squared sample correlation coefficient better than 0.7.

The jagged continuous line is the result of a band average of the discrete points. Figure 4b shows the same average line, together with the Q factors calculated from the fitted poles as in Figures 2 and 3. To give two different perspectives on any trends in the data, Figure 4a uses a logarithmic frequency scale while Figure 4b uses a linear scale. The remarks made above about the unreliability of residue phases can be echoed here about the corresponding Q values. Only a few strong poles (large plot symbols)

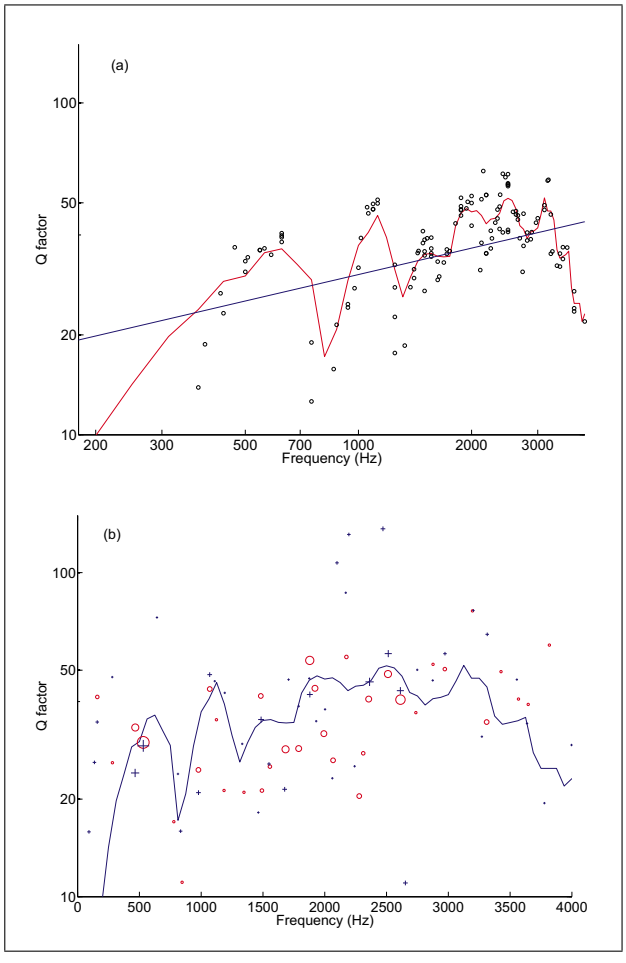

Figure 4. (a) Effective Q factors for the test violin determined from sonogram analysis as described in the text (circles), with band-average (jagged line) and regression line for power-law behaviour (straight line); (b) averaged line as in (a) but on a linear frequency scale, with values from the pole-residue fitting for the best case with complex residues (circles) and the best case with real residues (crosses).

close to the average line show reasonable consistency between the two fits. However, the general rising trend of the damping fit from Figure 4a, at least up to 3 kHz or so, is echoed recognisably in the spread of modal points.

The results of Figure 4 show interesting structure. There is a hint of a rising trend of Q factor with frequency, and also considerable local variation. Variation of Q factors is to be expected from the anisotropic properties of the wood of which the violin is made. For the typical woods used to make violins, it is well documented that the damping of bending vibration is much higher in the cross-grain direction than in the long-grain direction (see e.g. [31]). Modes of the complete violin body will combine these disparate damping factors in different proportions depending on the mode shape [32], leading to a spread of modal Q factors. There may also be underlying frequency variation of the material damping. Finally, there will also be variations in radiation damping among the modes, especially at lower frequencies.

The damping trend line looks somewhat linear in the log-log plot of Figure 4a, so a least-squares straight line has been fitted, also shown on the plot. This gives a power law for Q factor of the form $Q \propto f^{0.26}$. Similar power-law fitting of damping results for violins has been done by Bissinger on the basis of modal fits [33]. He obtains a mean power over a number of measured violins of 0.34, somewhat comparable to the value fitted here. However, it is far from clear that a power-law fit like this has any real significance for the underlying physics of damping: it could be argued that Figure 4b on a linear scale is equally suggestive of the constant value $Q \approx 40$. Further examples of damping trends will be shown and discussed in section 4.1.

3.3. Statistical results

The final stage of analysis is statistical. The first step is to average the measured admittance to estimate $Y_{\mathrm{dir}}(\omega)$ from equation (7). A Hanning window was used, to minimise visual artefacts as the edges of the window pass through strong features. Figure 5 shows the real and imaginary parts of the result, using an averaging bandwidth of 1000 Hz. The result is striking: it is immediately reminiscent of the complex response of a two degree of freedom system with resonant frequencies around 1700 and 2500 Hz. The real part stays positive, and shows a peak at the "resonances", while the imaginary part tends from positive towards negative values around the same frequencies.

This simple averaging procedure has given a rather direct visualisation of a feature of violin response that has been called the "bridge hill" [29, 34], a kind of local resonance involving the mass and stiffness properties of the violin bridge and also the region of the violin top between the f-holes where the bridge sits: Cremer [35] called this region the "island". The wide bandwidth of the peaks comes from radiation damping as energy flows out from the bridge feet into the body. This particular violin seems to show a double "hill": more examples and some discussion will be given later. It is quite logical that any local resonance near the point where the energy is being injected into the violin body should appear strongly in a quantity that represents the "infinite system" response. The averaging process has suppressed the body resonances that depend on the global configuration of the violin body, exactly as it was intended to do.

Next come the "SEA" quantities. The modal overlap factor can be calculated with the minimum of assumptions from equation (19), and also from the combination of equations (10) and (16). Both results for the sample violin are plotted in Figure 6. The two estimates are gratifyingly close, giving some confidence in the self-consistency of the results. The modal overlap rises at low frequencies, as expected, reaching the value $m = 1$ around 1200 Hz. This is consistent with earlier estimates, e.g. [36]. The overlap factor reaches a peak around 2 kHz, then declines somewhat before rising again. A falling trend of overlap factor seems quite unlikely on physical grounds, and it should be

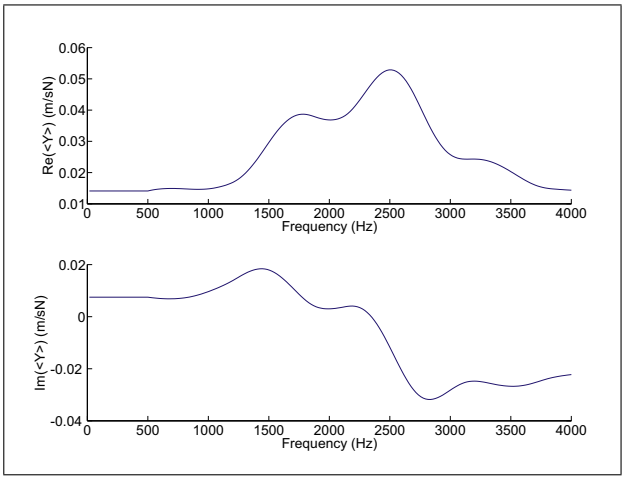

Figure 5. Band-averaged admittance $\langle Y \rangle$ for the test violin to estimate Y_{dir}.

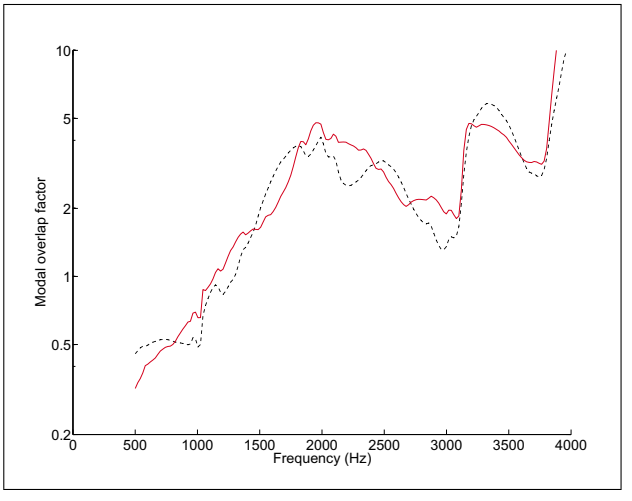

Figure 6. Modal overlap factor for the test violin estimated using equation (19) (solid line) and equations (10), (16) (dashed line).

said that the results from a range of instruments show significant differences of form above 2 kHz or so. More will be said on this issue in section 3.4.

Combining the modal overlap with the averaged damping from Figure 4 gives the modal density, shown in Figure 7. What is actually plotted is a slightly more intuitive quantity, the mean modal spacing expressed in Hz. Again, two estimates are shown, based on equation (19) or equation (16), and the two are in good agreement. The large fluctuations in the low-frequency portion of the plot derive mainly from the fitted damping curve, since the modal overlap showed relatively smooth variation in that range. Note from Figure 2a a common feature of violin response: a deep antiresonance around 700 Hz, roughly where Figure 7 shows a high value of modal spacing. Perhaps there really are fewer modes in this frequency range, so that the spacing is higher?

The horizontal lines in Figure 7 show the average spacing according to the various pole-residue fits, covering a considerable range as was evident from Figure 1. The SEA estimate gives a significantly lower spacing (or higher

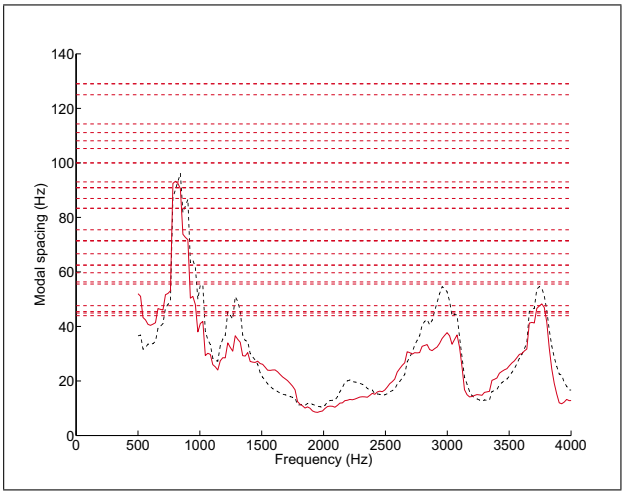

Figure 7. Mean modal spacing for the test violin estimated using equation (19) (solid line) and equations (10), (16) (dashed line). Horizontal dashed lines: estimates from fitted poles.

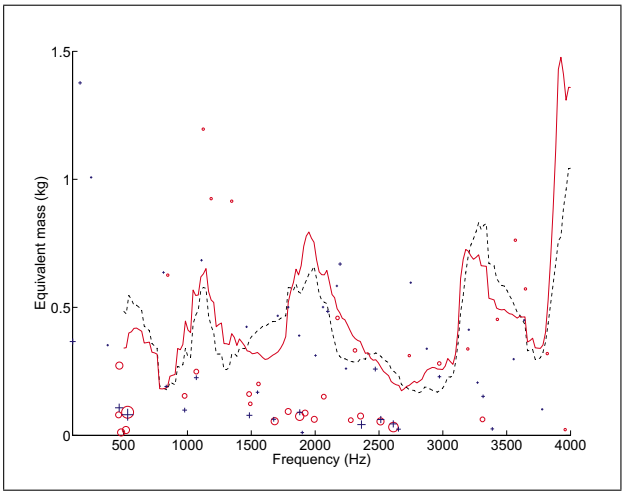

Figure 8. Effective mass for the test violin estimated using equation (19) (solid line) and equations (10), (16) (dashed line), with modal masses from the pole-residue fitting: best fit with complex residues (circles), best fit with real residues (crosses).

modal density) than the typical pole count from mode fitting. It is important to note that the SEA estimate of modal density, at least when applied to a homogeneous system, includes *all* modes and not only modes that give large peaks at the particular measurement position. The "missing" modes are included via an influence on the modal amplitudes. As a simple example, if a pinned-pinned rectangular plate is measured at its centre, only 25% of the modes will be seen because the others are antisymmetric in one or both central axes of the plate and so the measurement point lies on a nodal line. But the amplitudes of the doubly-symmetric modes that *are* seen in the measurement are all unusually large because the measurement is exactly at an antinode, and this produces a factor of 4 in the estimate that exactly compensates for the missing modes. On the other hand, given the acceptance criteria imposed on the pole fitting it is no surprise that this method might underestimate the number of modes since large peaks will have been fitted but small ones may have been missed. Directly counting visible peaks in the measured admittance at lower frequency where the modal overlap is fairly low suggests a mean spacing of the order of 50 Hz, comparable to the lowest values from counting fitted poles. Some light will be shed on this question in the next subsection, by comparison with results for a synthesised system.

Figure 8 shows the estimated total mass, again using the two approaches. Superimposed here are effective masses deduced from individual modal fits. It may be noted that a typical violin (without chinrest) weighs of the order of 0.4 kg, broadly consistent with the general trend of the results here. The "total mass" involved in the vibration might be expected to be rather less than the full weight, since the apparent mass deduced from vibration measured at the bridge will probably not be influenced a great deal by the mass of the neck, fingerboard, pegs etc. It is no surprise that the effective masses of the strong low-frequency modes are lower than any estimate of the total mass. The main deformation of these modes will presumably be concentrated in the low-mass parts of the violin body, especially the top plate.

3.4. Comparison with synthesised results

For a first indication of how these statistical results should be interpreted, it is useful to see what the analysis predicts for a system that is generically similar to a violin but whose properties are known in advance. For this purpose it is convenient to use a model developed in earlier work [29], which represents a crude "cigar box violin". Rigid rectangular "ribs" support two pinned-pinned flat rectangular plates with plan dimensions 321 × 204 mm^2, having approximately the properties of a spruce and maple violin top and back plate. All modes of both plates were given fixed damping with $Q = 30$. A rigid, massless "soundpost" connects the two plates, and the top plate is driven through a single-degree-of-freedom bridge model. The exact values of the model parameters do not matter very much here, but are all listed in Table I of [29]. The computational details are also described in that paper, and many examples are shown there of the predicted behaviour under various parametric changes.

The synthesised bridge admittance was analysed using the same process described earlier, without in this case requiring any compensation for added damping from strings. The modal fitting was found to work well, but even with this noise-free input data it still showed evidence of ill-conditioning similar to the results seen above for the real violin measurement. The damping trend fit reproduced the constant-Q behaviour accurately. Band averaging to reveal $Y_{\mathrm{dir}}(\omega)$ gave the result shown in Figure 9, which should be compared to Figure 5. A clear and prominent bridge hill is seen around 2.8 kHz.

Figure 10 shows the predicted modal overlap factor in the same format as Figure 6, with the average trend from the known mean modal density and damping superimposed. This shows that the expected trend is followed,

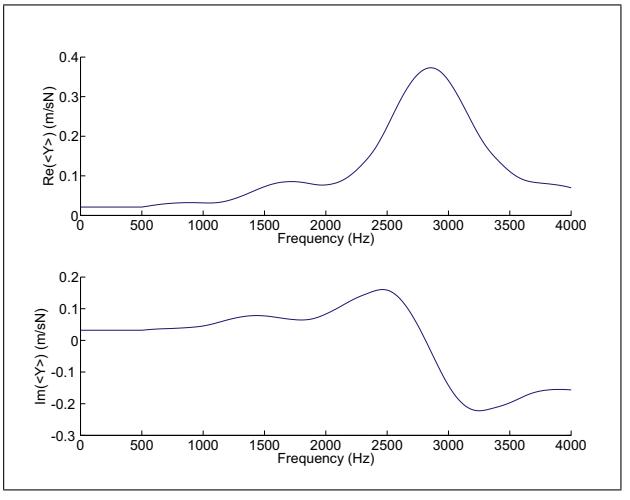

Figure 9. Band-averaged $\langle Y \rangle$ as in Figure 5 for the synthesised "cigar box violin" as described in the text.

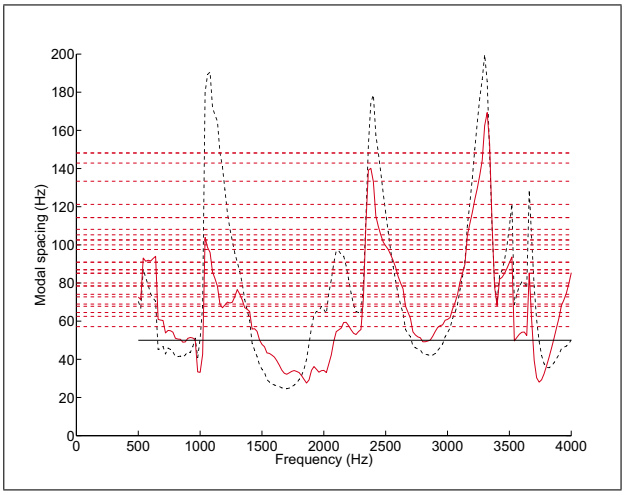

Figure 11. Estimated modal spacing as in Figure 7 for the synthesised "cigar box violin", with values from the pole fitting (straight dashed lines) and the exact mean answer (straight solid line).

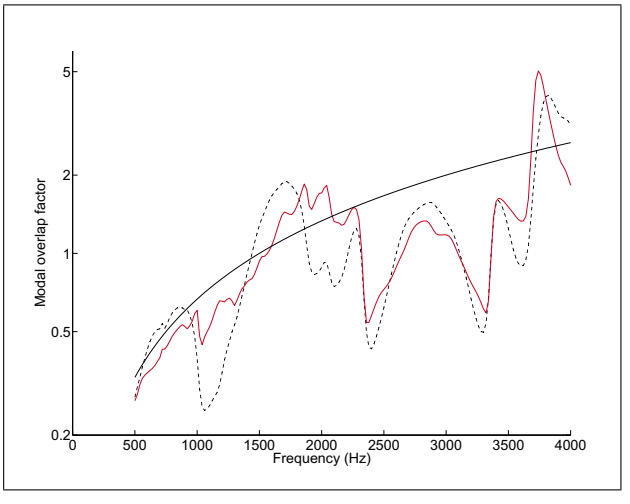

Figure 10. Estimated modal overlap factor as in Figure 6 for the synthesised "cigar box violin", with predicted trend from average modal density and known constant damping.

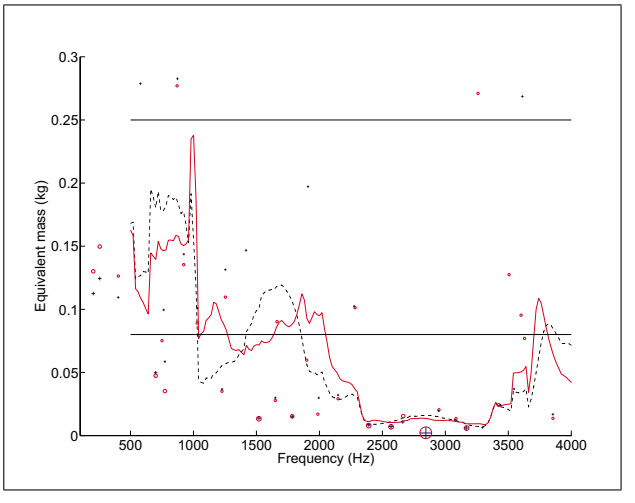

Figure 12. Estimated effective total mass as in Figure 8 for the synthesised "cigar box violin", with actual top plate mass (lower line) and total vibrating mass (upper line). Discrete points show values from the pole-residue fitting in the same format as Figure 8.

within a factor 2 or so, by both estimated curves up to about 2 kHz. Above that, the curves deviate significantly below the expected trend, in a shape that is reminiscent of the violin measurement in Figure 6. Tentatively, these plots can be interpreted as suggesting that the SEA-based estimates predict the correct trend until the frequency range where the "bridge hill" begins to have an influence. However, the simple theory used to derive the estimates, from section 2.3, does not take account of deterministic features like the bridge hill, and it is not surprising that some discrepancies appear in that frequency range. A more sophisticated treatment is needed to cope with this issue: for example, there is an extension of the SEA variance theory to hybrid systems with deterministic features [20], but this lies beyond the scope of the present paper. Notice that the height of the peak in Figure 9 is considerably greater than was seen for the test violin in Figure 5: the "cigar box" with these particular parameters has a rather over-the-top bridge hill, and that results in a particularly strong influence on the SEA estimates.

Figures 11 and 12 show the predicted modal spacing and effective total mass for the synthesised model, to be compared with Figures 7 and 8. The true average modal spacing is marked in Figure 11: it lies below any of the estimates based on pole-residue fitting, and follows reasonably closely the general level of the prediction curves. There are significant peaks and dips in the curves, though. It would need further detailed analysis to establish whether these are capturing genuine variations in the detailed distribution of natural frequencies: this would be an interesting question for future research. In Figure 12, two physical masses are marked as horizontal lines: the top plate mass

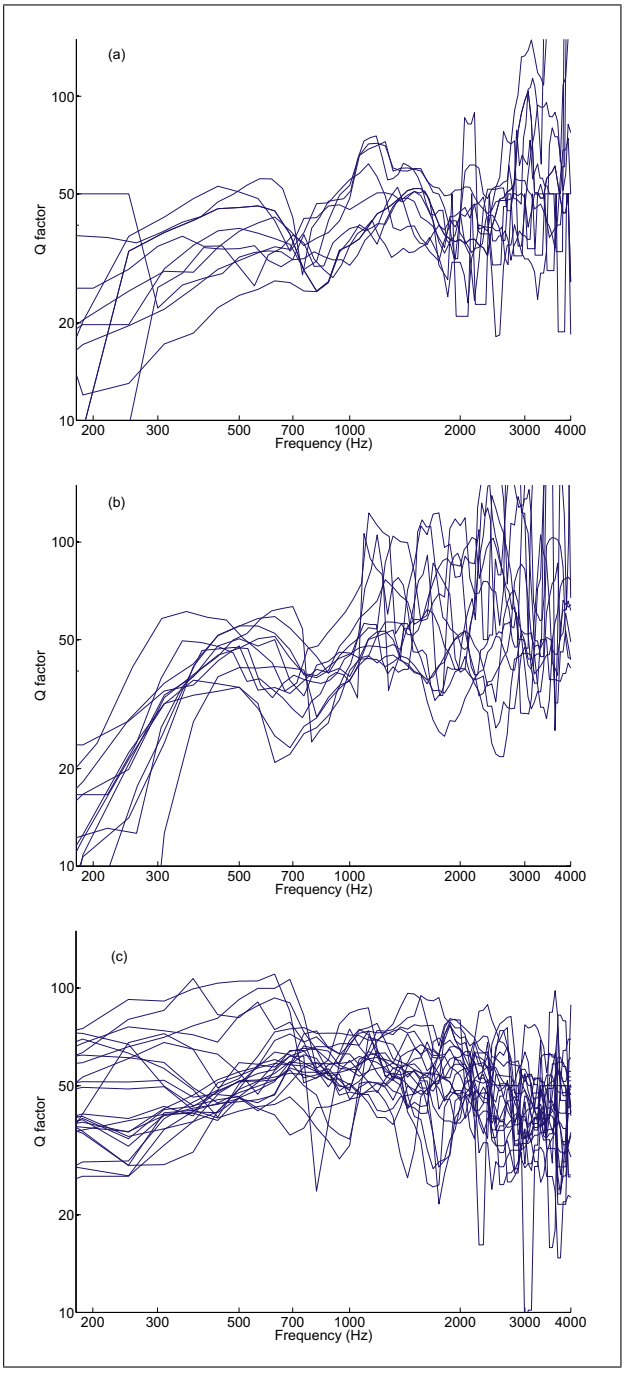

Figure 13. Damping trends as in Figure 4, for representative sets of (a) 11 modern violins; (b) 12 old violins; (c) 24 guitars.

0.08 kg and the total mass 0.25 kg. The predicted curves give a value intermediate between the two at low frequencies, then settle to values close to the top plate mass until 2 kHz. Above that, very low values are predicted in the frequency range already noted in Figure 10 as the range where the bridge hill has a significant influence. The very low mass of the dynamic bridge model (0.5 g), together with the very strong bridge hill, is presumably biasing the estimate based on a local "measurement" at the position of that mass. Again, it would be an interesting question for future research to explore the circumstances when analysis of this kind reveals global properties of an inhomogeneous system and when it gives local properties (such as the top plate mass in this example).

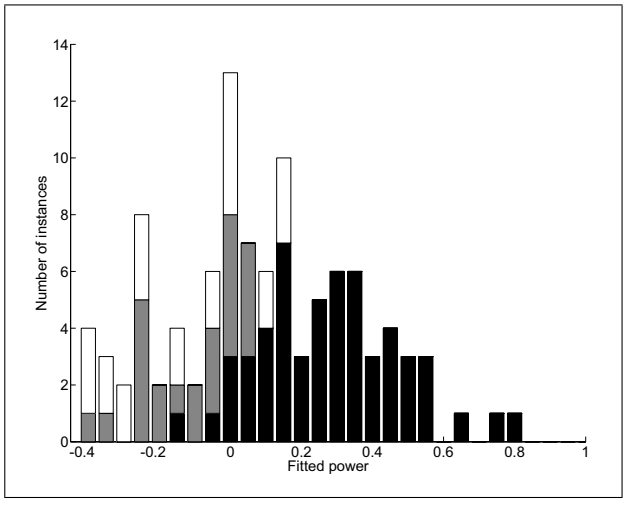

Figure 14. Histogram of best-fitted power-law exponent for the damping trend of violins (black); guitars (gray); viols (white).

4. Comparing instruments

The analysis just described has been applied to a set of around 150 measurements on the bodies of different stringed musical instruments. There are many possibilities to look for similarities and differences among these instruments, and space does not allow very many of these to be explored here. Two particular issues will be discussed to illustrate the scope. These draw upon two aspects of the analysis that are novel, and therefore reveal structure not previously accessible. Finally, some results will be shown to explore the repeatability of SEA estimates.

4.1. Damping results

The damping trend deduced from time-frequency analysis and illustrated in Figure 4 reveals unexpected differences between types of instrument. Figure 13a shows the trend line for a selection of 11 modern violins, while Figure 13b shows the same information for 12 old violins, including ones by Stradivari and Guarneri del Gesu. Figure 13c shows corresponding results for 24 acoustic guitars. The violin data were all obtained by George Stoppani, using a small accelerometer as the sensor, while the guitars were measured by the first author using a laser vibrometer. Other measurement details were as described in section 1. All three sets show some spread between individual instruments, but it appears that the violin data cluster around a different average trend than the guitar data. The old and modern violins show broadly similar behaviour, but if anything the old ones show lower damping at high frequencies: there seems to be no evidence here for systematically higher damping in old instruments, as was mooted earlier.

One way to make the difference between the violins and the guitars quantitative is via power-law fitting as illustrated in Figure 4a. Figure 14 shows a histogram plot of the

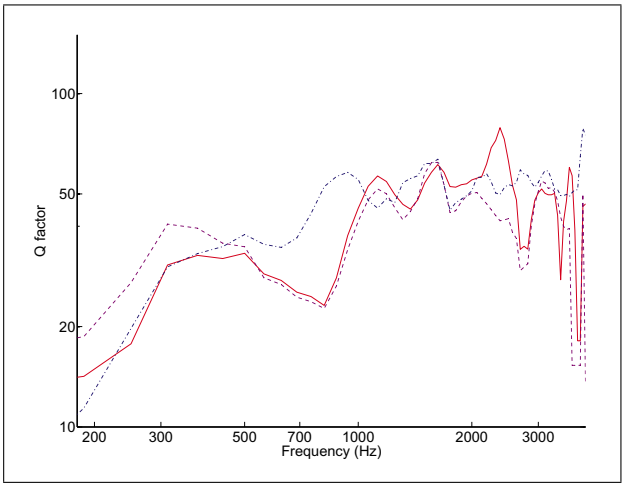

Figure 15. Damping trend as in Figure 4 for a violin with afterlengths undamped, compensated for one string polarisation (solid line); the same violin with afterlengths damped, compensated for both string polarisations (dashed line) and the rotational admittance for the violin body with strings and bridge removed, without compensation (dash-dot line).

best-fitted power, for an extended set of 55 violins in black, the set of 24 guitars in gray, and a set of 30 viols of assorted sizes and styles in white. All but two of the violins give a positive power, corresponding to the rising trend visible to the eye in Figures 3a,b. The mean power is 0.30, quite similar to the value 0.34 reported by Bissinger from a very different measurement and processing procedure [33]. For the guitars, by contrast, most show negative powers, and the mean is -0.09. To the eye, the trend of Figure 13c does not really resemble a straight line at all: it rises to a broad maximum around 1 kHz, then falls at higher frequencies. The numerical values of the fitted powers are probably not at all strongly associated with any underlying physics, they simply give an indication of differences in overall trend.

Why should violins and guitars show this systematic difference? In terms of factors that seem likely to influence damping behaviour, they have rather similar construction. Both are boxes made of thin wooden panels firmly glued around the edges. Both have soundholes, to create a Helmholtz-like resonance to boost sound radiation for the lowest notes in the played range. The typical materials used are somewhat different: violins almost invariably have their backs and sides made of maple (Acer pseudoplatanus) and their tops made of spruce of one kind or another, usually Picea abies. Guitar tops may be of similar spruce, but the set shown here includes examples with cedar and plywood tops. The backs and sides of guitars can be made from a wide variety of woods: Indian and Brazilian rosewood, maple, cypress and plywood are all represented here. The guitars show similar trends in Figure 13b despite this range of materials, including two that are made of spruce and maple of the same kind as a typical violin. This makes it very unlikely that the different trends are associated directly with material behaviour.

This seems to leave only two possibilities: the different damping trends are associated either with a difference of radiation damping, or with the mechanical effect of some structural difference, such as the frictional contacts in the violin associated with the bridge feet and the soundpost. Certainly there will be differences of detail in the sound radiation between violins and guitars: the size is different, for a start. But it is not easy to see how this would account for the apparent contrast at moderately high frequency, around 1–3 kHz: the Q factors of the violin seem to increase with frequency while those of the guitar decrease. If the underlying material damping is similar for both, the radiation damping of the guitar would need to be progressively rising relative to the violin to produce the trend in total damping. It is not obvious how this would be compatible with the usual pattern for radiating structures, where the radiation efficiency tends to a plateau around unity at higher frequencies. There could perhaps be a systematic difference in critical frequency, but guitar plates and violin plates are of similar thickness: guitars are perhaps on average a little thinner, compensated by additional bracing. The notion of "critical frequency" for strongly anisotropic materials like spruce is somewhat ambiguous, but for any plausible interpretation of the word, violins and guitars should have broadly similar values.

One feature of violin construction that might be relevant concerns the stringing: guitar strings are usually terminated at the bridge, but violin strings continue behind the bridge and terminate at the tailpiece. It was pointed out in section 2.2 that the vibration of the string afterlengths can play a role in the effective damping. The violin measurement that formed the basis of section 3 had the afterlengths damped, but this problem was not appreciated in the early years of bridge admittance measurement and many of the violins included in the results of Figures 13 and 14 were measured with undamped afterlengths. Might this perturb the results and give a bias to the damping trend?

It is straightforward to obtain direct information on this question. A violin (a different one from the results in section 3) was measured with afterlengths damped and undamped. Then the strings and bridge were removed, and measurements made directly on the body at the bridge-foot positions. To give a measure that is comparable, to an extent, to the bridge admittance the 2 × 2 matrix of body measurements were combined to calculate the "rotational admittance" $R = Y_{11} + Y_{22} - Y_{12} - Y_{21}$, introduced in an earlier study of the "bridge hill" [29]. The damping trends from these three measurements are plotted in Figure 15. The two bridge measurements were both compensated for the effect of highly damped strings as explained in section 2.2: but one is compensated for one polarisation only, while the other is compensated for both string polarisations. The body measurements were not compensated since the strings were absent. The difference between damped and undamped afterlengths is quite small until the feature around 2.4 kHz, which is an afterlength resonance. Another can be seen around 3.7 kHz.

An intriguing feature of Figure 15 is that direct body measurements produce generally higher Q factors than the measurement with damped but compensated strings and afterlengths. One might have guessed that the compensation was a bit too generous, since it assumes perfect damping of the strings, so that the Qs would come out higher than the body alone. However, the opposite is seen here, even for the case compensated for both string polarisations. Possibly the body damping is somewhat reduced by removing the strings and bridge, but it is far from clear why, and no systematic investigations of such effects have yet been made.

It does not seem likely from Figure 15 that an effect of afterlengths is the primary reason for the difference in damping trend between the violins and the guitars. This conclusion is reinforced by the results for viols, also shown in Figure 14. The viols measured for this set are much more disparate than either the violins or the guitars: sizes, shapes, number of strings, presence or absence of a soundpost, bridge design and many other constructional details are not at all standardised. Nevertheless, all the viols are strung with afterlengths and a tailpiece, and all were measured without damping the afterlengths. Despite this, the results for the power-fitting on the viols look much more like the guitars than the violins.

4.2. Which instruments show a bridge hill?

The second set of comparative results concerns the band-averaged admittance computed as an estimate of the "infinite-system" response $Y_{\mathrm{dir}}(\omega)$. As was shown in Figure 5, this gives a clear visualisation of any resonant behaviour in the immediate vicinity of the bridge, where the energy is being injected to the instrument body. For the test violin it showed a bridge hill peaking at around 2.5 kHz, with perhaps a second "hill" around 1.7 kHz. The "hill" feature has been extensively investigated in recent years (e.g. [29, 34]). It is of direct interest to instrument makers and adjusters, since it can give a resource for tonal adjustment of an instrument, either at the design stage by changes in the "island" area between the f-holes, or later by adjustments to the bridge.

Figure 16a shows results comparable to Figure 5 for three different violins. The solid line (a violin by Andrea Postacchini) shows a single peak around 2.2 kHz. The dashed line (a violin by Sam Zygmuntovicz) shows a peak at a much lower frequency around 1.6 kHz, and the dash-dot line (a violin of innovative lightweight design by Joseph Curtin) shows a very clear double peak as well as a much higher peak level. The double peaks are very intriguing, and probably indicate the presence of more than one local resonance in the island region. If the underlying physics could be established, the second peak might offer makers a further resource for tonal design and adjustment.

Figure 16b shows comparable results for three viols. In all cases the magnitudes are smaller than for the violins. The solid line shows a baroque treble viol by Norman Myall, which has a soundpost broadly similar to the violin. The dashed line shows a renaissance treble viol by Richard Jones, with no soundpost. The dash-dot line shows a speculatively reconstructed renaissance treble viol of "Costa" pattern made at West Dean College, without a soundpost. Of the three, only the Myall instrument has a feature resembling a "normal" bridge hill: there is a broad peak around 1.3 kHz showing the expected real/imaginary behaviour as in Figure 5. The Jones instrument perhaps shows two or even three peaks, widely spread across the frequency range. The Costa instrument shows as many as four peaks. Extensive further work would be needed to es-

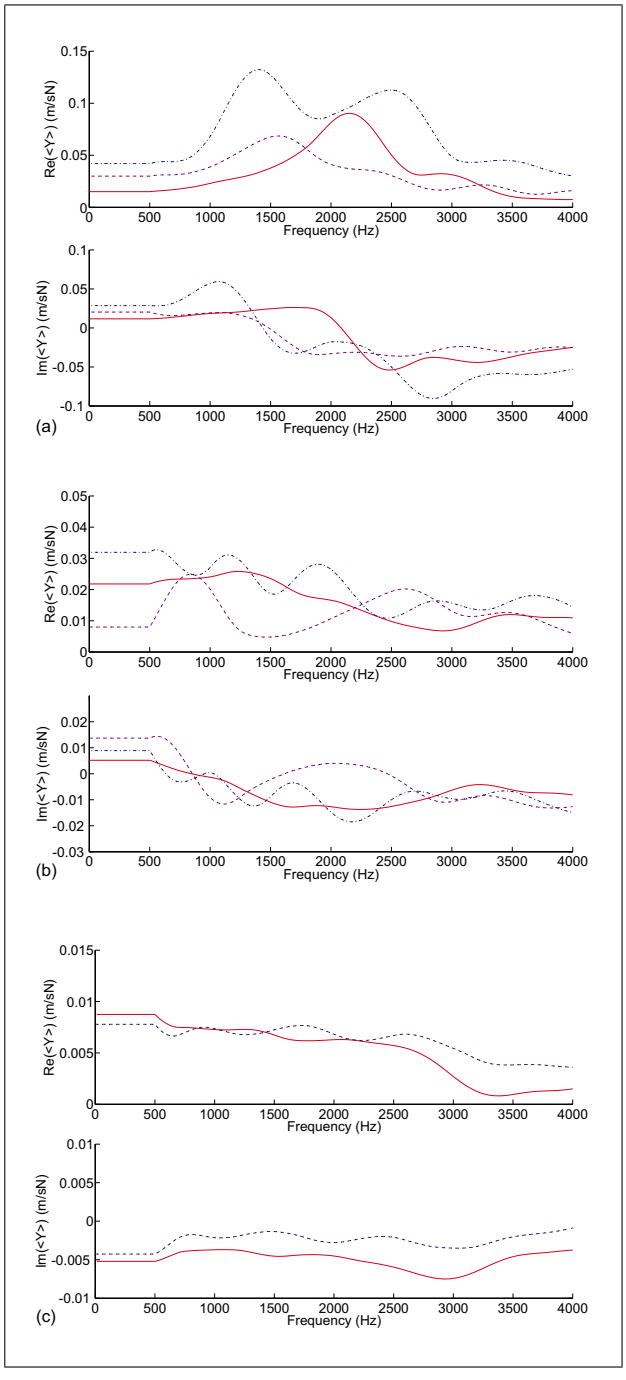

Figure 16. Band-averaged $\langle Y \rangle$ as in Figure 5 for (a) three violins; (b) three treble viols; (c) two guitars. Note that the vertical scales are different in the three cases.

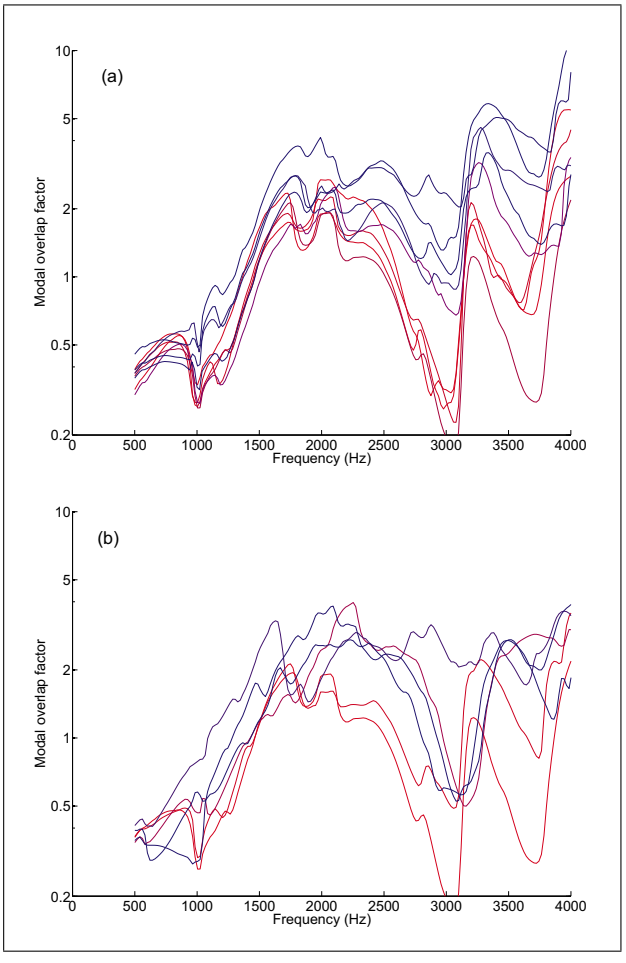

Figure 17. Modal overlap factor estimated from equation (18), for (a) multiple retests of a single violin over a period of 10 years; (b) six violins by the same maker (David Rubio).

tablish the significance of these peaks and whether the differences revealed are of musical importance.

Finally, Figure 16c shows results for two typical guitars: a flamenco guitar by Martin Woodhouse (solid line) and a classical guitar by Michael O'Leary (dashed line). The results are similar for both. The typical amplitudes are an order of magnitude smaller than the violin results. The behaviour is somewhat like that of an infinite plate, at least at lower frequencies: positive real part with roughly constant magnitude, and imaginary part much smaller. There seems to be no feature in a conventional guitar comparable to the bridge hill of the violin.

4.3. Reliability of modal overlap estimates

As a final example some results are shown to explore the reliability of SEA estimates. Figure 17 shows results for modal overlap factor, comparable to Figure 6. A set of violins made by David Rubio for the purposes of acoustical investigation are used. They have similar materials and overall design, but very significant differences in plate graduation so that the free-plate mode frequencies cover about as wide a range as is possible with a standard violin [37]. The violins from this set have been repeatedly tested over a period of years.

Figure 17a shows results for one of the violins measured on 9 different occasions over a decade: this is the same violin used in section 3. The local temperature and humidity will have varied, and there will have been gradual settling of the instrument. Strings, soundpost and bridge will all have changed during this time. The results show very similar patterns. The early measurements cluster together, and all show a dip around 3 kHz. Later measurements seem to get systematically higher in this frequency range. At higher frequencies the results are spread over a large range, but all show a rather similar shape. Figure 17b shows the set of six violins, all measured on the same occasion. They all show similar behaviour up to about 2 kHz, then they spread out. Most have a rather level trend with a value around 2. The differences of shape are marked by comparison with the retest results of Figure 17a.

5. Conclusions

A range of different analysis techniques has been presented for extracting information from a measurement of input admittance (or drive-point mobility) on a structure, with particular emphasis on application to the bodies of stringed musical instruments. The analysis includes both deterministic and statistical techniques. The first approach is automated pole-residue extraction, as used for modal analysis. Next, a damping trend against frequency is obtained by an approach analogous to reverberation time tests in room acoustics. An impulse response is derived by inverse Fourier transform, then time-frequency analysis is performed and time decay rates within frequency bins fitted. Finally, statistical quantities are extracted using theoretical results from Statistical Energy Analysis and its recent developments. Modal overlap, modal density and effective mass are estimated, together with the "direct field" component of the energy flow near the excitation point.

Results have been shown for violins, guitars and viols. A corpus of some 150 measurements allows comparisons to be made between different families of instruments, and also between different instruments of the same general type. For the particular violin used to illustrate the full set of analysis results, the modal overlap factor was found to reach unity at around 1.2 kHz. The pole-residue fits became implausibly erratic around the same frequency: they showed poor reproducibility with different choices of analysis bandwidth and model order, and residue phases outside the range permitted for passive damped systems.

The damping trend for the violins showed, very approximately, power-law behaviour similar to that previously reported by Bissinger [33]. It was shown that damping results from this analysis method are likely to contain artefacts if the strings are not thoroughly damped, including the after-length strings between the bridge and tailpiece. The energy loss from well-damped strings is compensated during the analysis. When comparing instruments of different types, an unexpected divergence in damping trends

was seen. All violins tend to show a rising trend of Q factor with frequency over the range examined (up to 4 kHz). Guitars, by contrast, show a trend that rises to a broad peak around 1 kHz and then falls at higher frequency. Viols seem to be more like guitars than violins in this respect. It is far from clear what aspect of the violin is responsible for this unexpected behaviour: it does not seem to be an effect of constructional material.

The direct field, deduced by linear averaging of the input admittance over a suitable frequency bandwidth, reveals the "bridge hill" of the violin very clearly and directly. The method should also reveal any other comparable resonant behaviour close to the bridge, where the energy is injected into the body. Some violins show a double peak, and the underlying physics of this behaviour would be worth investigating in case it gives a controllable resource for tonal adjustment to violin makers. Guitars show no trace of any local resonant behaviour: the direct field looks strongly reminiscent of the behaviour of a simple flat plate. Viols fall in between the two cases: no peaks as strong as the ones in the violin, but traces of multiple peaks at higher levels than in the guitar. Viols are much less standardised in their design than violins, and this measurement may be showing variations which have some significance for differences of sound between instruments.

Statistical analysis based on the simplest possible application of SEA-like arguments gave plots that may require further research to interpret fully. Preliminary comparisons with a synthesised model having known properties suggest that the plots of modal overlap factor, mean modal spacing and effective mass may give directly useful information at lower frequencies, but that for the instruments that show features like the "bridge hill" the predictions as currently presented may be misleading once the frequency range of these features is reached. To address this question, the statistical analysis will need to be extended to encompass recent developments in vibration theory that allow such features to be taken into account.

The earlier remarks about differences between families of instruments point towards other avenues for future work based on the analysis presented here. Trends and differences identified by this kind of analysis give new raw material for the design of psychoacoustical tests. It would be of interest to establish thresholds of perception for parametric changes in the various analysed quantities. Such thresholds could be compared to the actual variation revealed by the measurements, and this could lead to a ranking order for the perceptual significance of different factors. A start has been made on this program, using data from these measurements alongside listening tests for guitar sounds [38].

Acknowledgement

Many people contributed to this investigation by making instruments and data available; particularly George Stoppani, Murray and Patsy Campbell, and Alison Crum. The authors also thank Colin Gough and an anonymous reviewer for valuable suggestions.

References

[1] J. Woodhouse: Plucked guitar transients: comparison of measurements and synthesis. Acta Acustica united with Acustica **90** (2004) 945–965.

[2] J. Woodhouse: On the playability of violins. Part II: Minimum bow force and transients. Acustica **78** (1993) 137–153.

[3] E. V. Jansson: Admittance measurements of 25 high quality violins. Acustica united with Acta Acustica **83** (1997) 337–341.

[4] K. G. McConnell: Vibration testing. Wiley, New York, 1995.

[5] H. A. K. Wright: The acoustics and psychoacoustics of the guitar. PhD Thesis, Cardiff University, 1996.

[6] C. Fritz, I. Cross, B. C. J. Moore, J. Woodhouse: Perceptual thresholds for detecting modifications applied to the acoustical properties of a violin. J. Acoust. Soc. Am. **122** (2007) 3640–3650.

[7] R. H. Lyon, R. G. De Jong: Theory and application of statistical energy analysis. Butterworth-Heinemann, Boston, 1995.

[8] R. S. Langley, V. Cotoni: The ensemble statistics of the vibrational energy density of a random system subjected to single-point harmonic excitation. J. Acoust. Soc. Am. **118** (2005) 3064–3076.

[9] S. Zygmuntowicz, G. Bissinger: Strad 3D. Zygmuntowicz. See web site http://strad3d.org/cms/, 2009.

[10] L. Cremer, H. A. Müller, T. J. Schultz: Principles and applications of room acoustics. Applied Science, Barking, 1982.

[11] G. Weinreich: Vibration and radiation of structures with application to string and percussion instruments. – In: Chapter 3 of Mechanics of musical instruments, CISM lecture series. Springer, Berlin, 1995.

[12] J. Woodhouse: Linear damping models for structural vibration. J. Sound Vib. **215** (1998) 547–569.

[13] D. Ewins: Modal testing: Theory, practice and application. Research Studies Press, Taunton, 2000.

[14] Lord Rayleigh: The theory of sound. Dover, New York, 1945. see Vol. 1 chapter 5.

[15] A. Srikantha Phani, J. Woodhouse: Experimental identification of viscous damping in linear vibration. J. Sound Vib. **319** (2008) 832–849.

[16] C. H. Hodges, J. Power, J. Woodhouse: The use of the sonogram in structural acoustics and an application to the vibrations of cylindrical shells. J. Sound Vib. **101** (1985) 203–218.

[17] X. Boutillon, G. Weinreich: Three-dimensional mechanical admittance: theory and new measurement method applied to the violin bridge. J. Acoust. Soc. Am. **105** (1999) 3524–3533.

[18] A. K. Belyaev, R. S. L. (eds): IUTAM symposium on the vibrational analysis of structures with uncertainties. Springer, Dordrecht, 2011.

[19] P. Bremner, R. S. Langley: A hybrid method for the vibration analysis of complex structural-acoustic systems. J. Acoust. Soc. Am. **105** (1999) 1657–1671.

[20] R. S. Langley, V. Cotoni: Response variance prediction for uncertain vibro-acoustic systems using a hybrid deterministic-statistical method. J. Acoust. Soc. Am. **122** (2007) 3445–3463.

[21] N.-E. Molin, A. O. Wahlin, E. V. Jansson: Transient wave response of the violin body. J. Acoust. Soc. Am. **88** (1990) 2479–2481.

[22] N.-E. Molin, A. O. Wahlin, E. V. Jansson: Transient wave response of the violin body revisited. J. Acoust. Soc. Am. **90** (1991) 2192–2195.

[23] R. H. Lyon: Statistical analysis of power injection and response in structures and rooms. J. Acoust. Soc. Am. **45** (1969) 545–565.

[24] R. S. Langley: Universal eigenvalue statistics and vibration response prediction. IUTAM Symposium on the Vibration analysis of structures with uncertainties, Dordrecht, 2011.

[25] L. H. Mehta: Random matrices. Academic Press, San Diego, 1991.

[26] V. Cotoni, R. S. Langley, M. R. F. Kidner: Numerical and experimental validation of variance prediction in the statistical energy analysis of built-up systems. J. Sound Vib. **288** (2005) 701–728.

[27] F. J. Fahy: Sound and structural vibration. Academic Press, 1985.

[28] O. Christensen, B. B. Vistisen: Simple model for low-frequency guitar function. J. Acoust. Soc. Am. **68** (1980) 758–766.

[29] J. Woodhouse: On the "bridge hill" of the violin. Acta Acustica united with Acustica **91** (2005) 155–165.

[30] K. Ege, X. Boutillon, B. David: High-resolution modal analysis. J. Sound Vib. **325** (2009) 852–869.

[31] D. W. Haines: On musical instrument wood. Catgut Acoust. Soc. Newsletter **31** (1979) 23–32.

[32] M. E. McIntyre, J. Woodhouse: On measuring the elastic and damping constants of orthotropic sheet materials. Acta Metallurgica **36** (1988) 1397–1416.

[33] G. Bissinger: Structural acoustics model of the violin radiativity profile. J. Acoust. Soc. Am. **124** (2008) 1764–1773.

[34] E. V. Jansson, B. K. Niewczyk: On the acoustics of the violin: bridge or body hill. J. Catgut Acoust. Soc. Series 2, 3, 7 (1999) 23–27.

[35] L. Cremer: The physics of the violin. MIT Press, Cambridge MA, 1984.

[36] J. Woodhouse: Body vibration of the violin Ů what can a maker expect to control? J. Catgut Acoust. Soc. Series 2, 4, 5 (2002) 43–49.

[37] J. Woodhouse: A set of violins for player-rating experiments. Proceedings of the Stockholm Music Acoustics Conference 1993,, Royal Swedish Academy of Sciences, 1994, 438–440.

[38] J. Woodhouse, E. K. Y. Manuel, L. A. Smith, A. J. C. Wheble, C. Fritz: Perceptual thresholds for acoustical guitar models. Acta Acustica united with Acustica **98** (2012) 475–486.